Design and Development of Pyrazole Schiff Bases Against MRSA: Synthesis, Spectral, and Biological Studies Infections

K.B. Chethan Kumar, Prabhudeva B.B, Y.B. Basavaraju
Department of Studies in Chemistry, University of Mysore, Manasagangotri, Mysore, 570 006, Karnataka, India

DOI*:* 10.64823/ijter.2601004

Date of Submission: Jan 21, 2026, **Date of Acceptance (Fast Track):** Jan 22, 2026, **Date of Publication:** Jan 23, 2026

Abstract: This study reports the design and synthesis of a series of pyrazole Schiff bases and their evaluation as potential antibacterial agents against methicillin-resistant *Staphylococcus aureus* (MRSA). The compounds were synthesized via condensation of pyrazole amines with aromatic aldehydes and characterized using FT-IR, NMR, and elemental analysis. Pharmacophore modeling and ADMET predictions indicated favorable pharmacokinetic properties. Among the synthesized derivatives, compound 7i showed the most promising results, with a docking score of -7.4 kcal/mol against the PBP2a enzyme of MRSA and a binding free energy of -42.8 kcal/mol from MM-GBSA calculations. Molecular dynamics simulations confirmed the stability of the 7i-PBP2a complex, while density functional theory (DFT) analysis revealed a HOMO-LUMO gap of 4.28 eV, indicating strong stability and reactivity. Antibacterial studies demonstrated that compound 7i exhibited a minimum inhibitory concentration (MIC) of 84 µg/mL and a zone of inhibition of 10 mm at 100 µg, highlighting measurable activity against MRSA. Compared with standard antibiotics, these results suggest that pyrazole Schiff bases, particularly compound 7i, represent a novel structural class with potential as lead molecules for the development of new anti-MRSA agents.

***Index Terms*:** Pyrazole Schiff base; MRSA; Molecular docking; Molecular dynamics simulation; Drug design.

I. INTRODUCTION

Methicillin-resistant *Staphylococcus aureus* (MRSA) is considered one of the most dangerous pathogens associated with antimicrobial resistance (AMR) [1]. It has become a serious clinical and economic burden worldwide. According to the World Health Organization, nearly 700,000 people die every year due to antibiotic-resistant bacterial infections, and by 2050 this number could rise to 10 million annually if proper medical measures are not taken [2].

S. aureus is responsible for a wide range of infections, and their treatment depends mainly on antibiotics that target essential bacterial processes such as cell wall synthesis, transcription, translation, and DNA replication. However, resistance develops rapidly through different mechanisms, including alteration of drug targets, enzymatic inactivation of antibiotics, enhanced efflux of drugs, and reduced uptake. This has created a major medical challenge, with high costs to both health and the economy [2]. The discovery of penicillin in the

1940s was a breakthrough in antibacterial therapy, but resistance soon emerged [3]. Methicillin, a semi-synthetic β-lactam introduced in 1959, also failed due to the emergence of MRSA [4]. Today, more than 90% of *S. aureus* strains are resistant not only to penicillin derivatives but also to many other antibiotics, such as aminoglycosides, macrolides, tetracyclines, chloramphenicol, and fluoroquinolones [5].

MRSA acquires resistance to antibiotics primarily through the mecA gene, which is transferred via horizontal gene transfer and encodes the PBP2a protein. This protein enables cell wall synthesis even in the presence of β-lactam antibiotics. Additionally, MRSA may use efflux pumps to expel antibiotics from the cells, produce enzymes like β-lactamases to degrade antibiotics, and accumulate genetic mutations that confer resistance to multiple antibiotic classes. These mechanisms collectively allow MRSA to survive treatment and pose a significant challenge in infection control [6]. The combination of efflux pumps, β-lactamase production, and genetic mutations makes MRSA one of the toughest pathogens to control [7].

Schiff bases are important in antimicrobial research because of their simple synthesis, versatile chemistry, and wide biological applications [7]. They can act as individual antibacterial agents or work synergistically with existing antibiotics to enhance activity. They are also able to target bacterial biofilms, which are often resistant to conventional therapy, making them valuable for infection control [8]. The era of heterocyclic-based antibacterial agents began with the discovery of penicillin, which targets cell wall synthesis by inhibiting the DD-transpeptidase enzyme. Although many researchers have developed derivatives of existing drugs, resistance has limited their effectiveness, highlighting the need for new drug candidates employing different mechanisms against MRSA [9]. Pyrazole derivatives are another well-known class of heterocyclic compounds with diverse pharmacological applications, including antibacterial [10], anticancer [11], anticonvulsant [12], antipyretic [13], antidepressant [14], and selective enzyme inhibition. Pyrazole moieties are already present in marketed drugs such as Apixaban, Celecoxib, Remogliflozin etabonate, Lonazolac, Fipronil, Tolpiprazole, and Deracoxib, which confirms their pharmaceutical relevance.

Although Schiff bases and pyrazoles have shown strong biological activities individually, their combination as pyrazole Schiff base hybrids has not been widely explored against MRSA. In our design, we hypothesized that introducing electron-donating or electron-withdrawing substituents on the benzylidene part of the Schiff base would influence antibacterial potential by modulating interactions with PBP2a. This structural approach is expected to generate new variants that may help overcome common resistance mechanisms. Based on this hypothesis, we synthesized and characterized a new series of pyrazole Schiff bases and studied their antibacterial activity against MRSA using spectral analysis, molecular docking, molecular dynamics simulation, ADMET, DFT, and MIC assays **(Fig. 1)**.

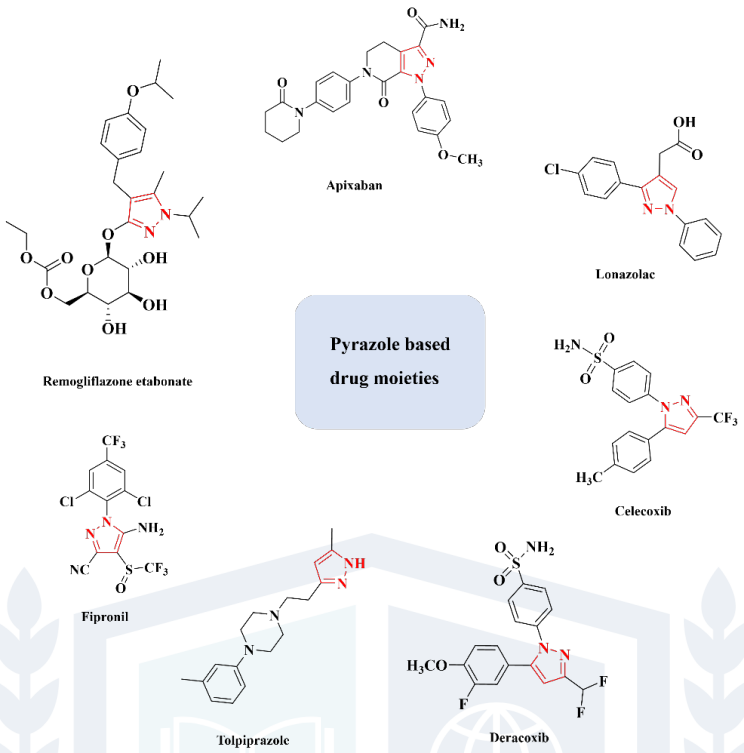

Fig. 1. Drug containing a pyrazole moiety.

II. MATERIALS AND METHOD

Chemicals and reagents were procured from Sigma Aldrich (Merck Pvt. Ltd., India). For column chromatography, Silica gel was purchased from Merck Pvt. Ltd. (Mumbai, India). TLC monitored the completion of the reaction. The FT-IR spectra were recorded on a PerkinElmer Spectrum Version 10.03.09. The ^{1}H and ^{13}C spectra (Agilent-NMR) were recorded using $CDCl_3$ as solvent. Chemical shifts were reported in parts per million relative to tetramethylsilane as an internal standard. A water micro TOF QII mass spectrometer was used to determine the Mass.

A. Synthesis of Pyrazole Schiff Bases

Pyrazole Schiff bases were prepared by reacting aromatic aldehydes with pyrazole amine in a minimum quantity of ethanol. A catalytic amount of glacial acetic acid was added to the round-bottom flask. Subsequently, the reaction mixture was refluxed for 4 hours **(Scheme 1)**. Progress and completion of the reaction were monitored by thin-layer chromatography using Ethyl acetate and n-hexane as the mobile phase. The product was precipitated by cooling the reaction mixture to room temperature, and then the precipitate was filtered and dried.

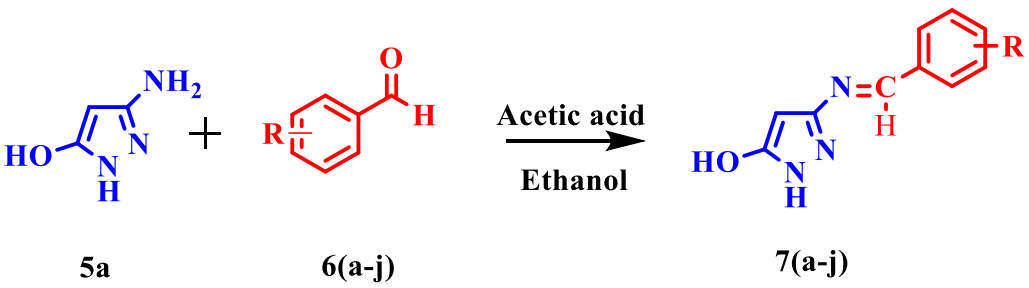

Scheme 1. Synthetic route for the synthesis of pyrazole Schiff bases.

7a. 3-(benzylideneamino)-1H-pyrazol-5-ol

FT-IR: 3542 (O-H), 2844 (C-H), 1612 (C=N). **^{1}H NMR:** δ 5.72 (1H, s, Pyr), 7.37 (3H, d, Ar-H), 7.94 (2H, d, Ar-H), 8.99 (1H, s, CH=N), 11.22 (1H, s,OH), 12.57 (1H, s, NH). **^{13}C NMR:** δ 123.8, 127.8, 128.4, 128.6, 135.6, 150.9, 160.0, 161.7. **Elemental Analysis:** Calculated: For: $C_{10}H_9N_3O$ (in %): C-64.16; H-4.85; N-22.45. Found:C-63.98; H-4.74; N-22.58.

7e. 3-((4-fluorobenzylidene) amino)-1H-pyrazol-5-ol

FT-IR: 3526 (O-H), 2894 (C-H), 1640 (C=N). **^{1}H NMR:** δ 5.62 (1H, s, Pyr), 7.22 (2H, d, Ar-H), 7.62 (2H, d, Ar-H), 8.54 (1H, s, CH=N), 11.08 (1H, s, OH), 12.14 (1H, s, NH). **^{13}C NMR:** δ 115.2, 130.4,132.1, 155.6, 158.2, 160.0, 165.1. **Elemental Analysis:** Calculated: For: $C_{10}H_8FN_3O$ (in %): C-58.54; H-3.93; N-20.48. Found: C-58.88; H-3.78; N-20.87.

7f. 3-((4-nitrobenzylidene)amino)-1H-pyrazol-5-ol

FT-IR: 3558 (O-H), 2920 (C-H), 1636(C=N). **^{1}H NMR:** δ 5.63 (1H, s, Pyr), 7.81 (2H, d, Ar-H), 8.31 (2H, d, Ar-H), 9.25 (1H, s, CH=N), 10.96 (1H, s, OH), 12.16 (1H, s, NH). **^{13}C NMR:** δ 123.8, 129.4, 135.6, 147.3, 150.9, 160.0, 161.7. **Elemental Analysis:** Calculated for $C_{10}H_8N_4O_3$ (in %): C, 51.73; H, 3.47; N, 24.13. Found:C-51.44; H-3.22; N-24.37.

7i. 3-((4-methylbenzylidene) amino)-1H-pyrazol-5-ol

FT-IR: 3527 (O-H), 2884 (C-H), 1664 (C=N). **^{1}H NMR:** δ 2.34 (3H, s, CH_3), 5.63 (1H, s, Pyr), 7.06 (2H, d, Ar-H), 7.24 (2H, d, Ar-H), 8.46 (1H, s, CH=N), 10.86 (1H, s, OH), 12.06 (1H, s, NH). **^{13}C NMR:** δ 21.3, 123.8, 128.5, 129.1, 135.6, 141.5, 150.9, 160.0, 161.7. **Elemental Analysis:** Calculated: For $C_{11}H_{11}N_3O$ (in %): C-65.66; H-5.51; N-20.88. Found: C-65.31; H-5.43; N-20.54.

7j. 3-((4-methoxybenzylidene) amino)-1H-pyrazol-5-ol

FT-IR: 3512 (O-H), 2908 (C-H), 1638 (C=N). **^{1}H NMR:** δ 3.79 (3H, s, OCH_3), 5.48 (1H, s, pyr), 7.24 (2H, d, Ar-H), 7.44 (2H, d, Ar-H), 8.64 (1H, s, CH=N), 10.64 (1H, s, OH), 12.14 (1H, s, NH). **^{13}C NMR:** δ 56.0, 114.3, 123.8, 130.1, 135.6, 150.9, 160.0, 161.7. **Elemental Analysis:** Calculated: For:$C_{11}H_{11}N_3O_2$ (in %):C-60.82; H-5.10; N-19.34. Found:C-60.74; H-5.24; N-19.48.

B. Pharmacophore Model

The anticipation of pharmacophoric features plays a crucial role in identifying the enhanced activity of synthesized pyrazole Schiff base compounds against penicillin-binding protein (PBP2a). In this study, the pharmacophore model was generated using the PHASE module implemented in Schrodinger. Numerous pharmacophoric features were identified around the active sites of the protein. From these, four key features were chosen to formulate a hypothesis regarding the ligand's interaction with the 1MWT protein.

C. ADMET Prediction

The ADMET screening was carried out for the five derivatives of the synthesized pyrazole Schiff bases to evaluate their pharmacokinetic properties. An ADMET (Absorption, Distribution, Metabolism, Excretion, and Toxicity) study is a comprehensive assessment of a drug's pharmacokinetics. This involves predicting the destiny of a drug and understanding the effects it induces within the body. Key aspects include determining the extent of drug absorption, particularly in oral administration and the gastrointestinal tract. This information is pivotal in comprehending the drug's behavior, potential neurotoxic and nephrotoxic effects, and overall disposition within the organism. In this work, ADMET predictions were performed using the pkCSM pharmacokinetics server (http://biosig.unimelb.edu.au/pkcsm/). This platform enabled the evaluation of

gastrointestinal absorption, blood–brain barrier permeability, P-glycoprotein substrate potential, cytochrome P450 inhibition profiles, and potential toxicity (including hepatotoxicity and nephrotoxicity). In essence, an ADMET study provides valuable insights into how a drug molecule is absorbed, distributed, metabolized, and excreted, as well as its potential for inducing toxicity. This comprehensive understanding is fundamental to the field of computational drug design, aiding in the identification and optimization of drug candidates during the drug discovery process.

D. Molecular Docking Studies

Molecular docking analysis was performed using MGL Tools 1.5.6 [15] and AutoDockVina [16], [17] to evaluate the inhibitory potential of the **7i** molecule against Penicillin G acyl-Penicillin binding protein 2a from Methicillin-resistant Staphylococcus aureus (MRSA). The three-dimensional X-ray crystal structure of the protein (PDB ID: 1MWT) was obtained from the Protein Data Bank (www.rcsb.org) in PDB format. Non-polar hydrogen atoms were incorporated into the protein structure using AutoDock Tools (ADT), followed by energy minimization for structural optimization and the removal of unfavourable contacts. The prepared protein structure was saved in PDBQT format, a format compatible with AutoDockVina for docking simulations. [18]. To identify the protein's active site, a grid box with dimensions of 60 Å (x), 60 Å (y), and 60 Å (z) was created, centered at coordinates (x=-36.765, y=46.021, z=66.777) to encompass the binding site. AutoDockVina 1.5.6 was used for the docking process, allowing the **7i** molecule to dock into the protein's active site. This algorithm explored various ligand conformations and predicted their binding affinities to the receptor. The interactions between the **7i** molecule and the protein were subsequently visualized and analysed using Biovia Discovery Studio 2019 visualizer. [19].

E. Molecular Dynamics Simulation

The dynamics simulation of a protein-ligand complex was performed using the academic version of the Desmond modules in the Schrodinger 2020-22 suite [20]. MD simulation setup: The purpose of the MD simulation was to assess the stability of the protein-ligand complex inside the active site of the targeted protein. The system was prepared by immersing TIP3P water molecules into an orthorhombic box. The water molecules were represented using a simple point-charge model. The OPLS3 force field was applied to parameterize and assess the complex, ensuring an accurate representation of the intermolecular interactions [21]. Compound introduction: A conjugated algorithm was employed to introduce the ligand compound into the system. This algorithm helps to position the ligand in a reasonable starting conformation, ensuring convergence with a threshold of 1 kcal/mol. This step is essential to properly initialize the ligand in the active site and allow it to interact with the protein. System relaxation: The relaxed system, including the protein-ligand complex and solvated water molecules, underwent energy minimization to remove any steric clashes and unfavourable contacts. This process helps to stabilize the system and achieve an energetically favourable starting point for the subsequent MD simulations. Molecular dynamics simulation: The system was subjected to 100 ns of molecular dynamics (MD) simulations. The simulations were performed in the NPT ensemble, maintaining a pressure of 1 bar using the Marryana-Tobias-Klein barostat. The temperature was kept constant at 300 K using the Nose-Hoover thermostat. These conditions simulate a realistic environment and allow the system to equilibrate and explore different conformations and interactions. Evaluation of stability and interactions: The stability of the protein-ligand complex and its interactions were assessed using the root mean square deviation (RMSD) and root mean square fluctuations (RMSF). RMSD measures the average deviation of the protein-ligand complex structure from the starting conformation throughout the simulation. RMSF provides information about the flexibility and fluctuations of individual residues within the complex. These analyses help to understand the dynamic behaviour and stability of the complex during the simulation [22].

F. MM-GBSA

The MM-GBSA method is commonly employed to calculate the binding free energy of complex systems. In this study, the Prime MM-GBSA module within the Desmond modules of the Schrodinger 2020-2 suite software was utilized to determine the binding free energy of the compound 7i when bound to the PBP2a protein [23]. The use of an MD simulation trajectory enhances the accuracy of the MM-GBSA calculations compared to other scoring functions. [24]. This approach allows for a more comprehensive analysis of the protein-ligand complex and provides valuable insights into the thermodynamics of binding. [25].

G. Quantum Computational Analysis

The structural geometry of the **7i** molecule was optimized and its energy was calculated using DFT with the 6-311++G(d,p) basis set in Gaussian 09 [26]. The DFT calculations employed a three-parameter hybrid exchange function and the LYP correlation function. [27]. Frontier molecular orbitals (FMOs) and molecular electrostatic potential (MEP) were derived from the optimized geometry. The estimation of FMOs, their energy gap, and related global reactive parameters was done using Koopman's approximation. [28]. Visualization of FMOs was conducted with GaussView 6.0 software [29].

H. Antimicrobial Studies

Methicillin-resistant *Staphylococcus aureus* (MRSA) strain ATCC43300 was employed in antimicrobial assays for both minimum inhibitory concentration (MIC) and zone inhibition by the broth dilution method and disc diffusion method. [30].

- **Broth Dilution Method for Determination of the MIC**

The MRSA cultures were grown in particular broths for 16-18 h at 37°C to obtain cell suspensions. The cell density was adjusted to 1 × 10^6 cells/mL using a McFarland Standard of 0.5. Stock solutions of the appropriate concentration (100 mg/mL) were then prepared in suitable solvents and diluted with media (2X) to obtain the final concentrations indicated by the dilution series. Synthesized compounds had different doses ranging from 1 mg/mL for each mL of 0.5, to 0.015 mg/mL, and Clindamycin's drug concentration, analysed was (8 µg/mL: 8 to 0.125 µg/mL) was prepared in Mannitol salt broth. Synthesized compounds were not added to the control (mannitol salt) broth during the inoculation process. Potato dextrose broth without any medication was prepared in control wells, while 90 µL of test samples/standards of various concentrations were combined with 10 µL of inoculum in 96-well plates. The OD values were measured at an optical density of approximately 590 nm after 24 hours of incubation at 35°C. The colour was changed from blue to pink when resazurin solution (0.015%) was added to each well and further incubated for another 4-6 hours, turning it into a purple-blue color. The highest MIC value detected in the dilution series was considered the concentration of MIC [31], [32].

- **Disc Diffusion Method for Determination of Zone of Inhibition**

Synthesized compounds were assessed for the zone of inhibition using Mannitol Salt Agar with Oxacillin from Himedia against MRSA. Inocula were prepared from bacterial cultures grown in respective broths at 37°C for 16-18 hours, with cell density adjusted to $1x10^6$ cells/ml using the 0.5 McFarland Standard. Growth requirements indicated that the organism is a facultative anaerobe in mannitol salt broth as well as on plates. Synthesized compounds (100 mg/mL), including a sample and Clindamycin (0.1 mg/mL) as a standard, and DMSO control, were used. The agar plates (90 mm) were then screened with inoculum mixed with water to make them spreadable uniformly, and wells of about 5 mm in diameter were cut out from the surface of the agar plate aseptically. Then, these wells were loaded with synthesized compounds (5 µl, 10 µl, and 20 µl; each

at a concentration of 100 mg/mL) and Clindamycin (10 µl, concentration: 0.1 mg/mL). Incubation was conducted at 37°C for 24 hours, and subsequently, zones of inhibition were observed. [33].

III. Results And Discussions

A. Chemistry

The structure of the synthesized pyrazole Schiff base compounds was confirmed by different spectral techniques, FT-IR, ^{1}H-NMR, and HRMS. The theoretical values of the elemental analysis are in good agreement with the experimental values **(Table 1)**, which lie within ± 0.4 % [34]. FT-IR spectra were recorded using KBr pellets in the range of 4000-400 cm^{-1}. IR spectra of compound **7i** show that the band at 1664 cm^{-1} corresponds to the C=N vibration characteristic of imines, and the absorption band at 2884 cm^{-1} is due to aromatic C-H stretching [35], [36]. The ^{1}H-NMR spectra of the oxadiazole Schiff base were recorded using $CDCl_3$. Their peak multiplicity and integration assigned the expected resonances. The spectral integration shows good accordance with the synthesized Schiff bases. The ^{1}H-NMR peak at δ 9.25 ppm is due to the imine proton, which confirms the formation of the Schiff base [37]. The proton spectral data are in good accordance with the number of protons and their chemical shifts with the proposed structure. Mass spectra of the synthesized Schiff bases showed an M^+ fragmentation peak in agreement with their molecular formula [38].

Compound	Substituent (Ar)	Structural description	Molecular formula
7a	Phenyl (-C_6H_5)	3-(Benzylideneamino)-1H-pyrazol-5-ol	$C_{10}H_9N_3O$
7e	p-Fluorophenyl (-C_6H_4F)	3-((4-Fluorobenzylidene)amino)-1H-pyrazol-5-ol	$C_{10}H_8FN_3O$
7f	p-Nitrophenyl (-$C_6H_4NO_2$)	3-((4-Nitrobenzylidene)amino)-1H-pyrazol-5-ol	$C_{10}H_8N_4O_3$
7i	p-Methylphenyl (-$C_6H_4CH_3$)	3-((4-Methylbenzylidene)amino)-1H-pyrazol-5-ol	$C_{11}H_{11}N_3O$
7j	p-Methoxyphenyl (-$C_6H_4OCH_3$)	3-((4-Methoxybenzylidene)amino)-1H-pyrazol-5-ol	$C_{11}H_{11}N_3O_2$

Table 1. Summary of synthesized pyrazole Schiff bases and their substituents.

B. Pharmacophore Model

The resulting four-featured hypothesis comprised two acceptor groups, one donor group, and one aromatic ring group. The developed pharmacophore yielded approximately 14 modules with varied pharmacophoric features. Among the generated pharmacophoric features, the AHRRR (Acceptor, Hydrophobic, Ring Aromatic) five-featured model was deemed the most optimal based on the site score, as detailed in **Table 2**. This selected model, with its five features, effectively distinguished the synthesized compounds into active and inactive categories, employing fitness scores and volume scores (refer to **Table 2**). Notably, compound **7i** exhibited a commendable fitness score of 3. All five compounds (**7a**, **7e**, **7f**, **7i**, and **7j**) were subsequently subjected to ADMET analysis for further evaluation.

Compound	Vector score	Volume score	Site score	Fitness score	Structure	Docking score
Active						
7a	1	0.969	0.99	2.969	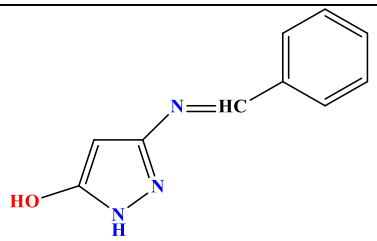	-7.0
7e	1	0.995	0.99	2.995	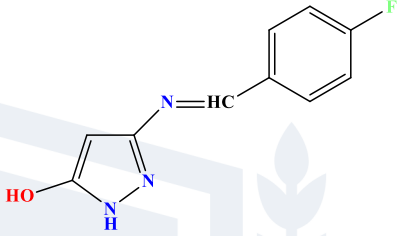	-7.2
7f	1	0.936	0.99	2.935	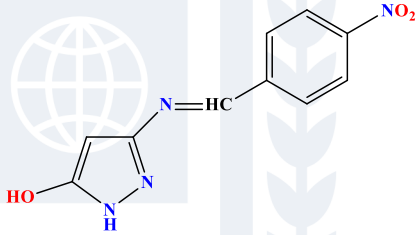	-7.2
7i	1	1	1	3	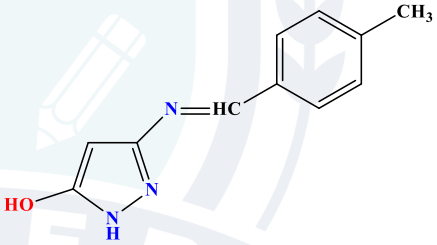	-7.3
7j	1	0.938	0.99	2.937	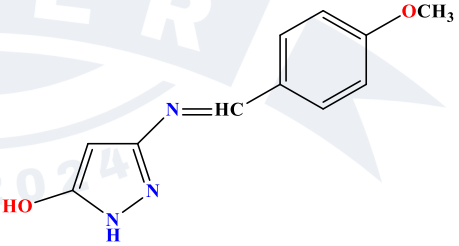	-7.1

Table 2. Pharmacophore Model results of novel synthesized pyrazole Schiff base compounds.

C. ADMET Prediction

The ADMET properties of the five derivatives exhibit notable similarities, prompting a meticulous evaluation and comparison of each property among the derivatives. Essential criteria for a compound to be considered for drug administration include low toxicity. Among the five compounds, **7a** and **7f** displayed AMES toxicity, leading to their exclusion from further assessment. Further analysis focused on the Oral Rat Chronic Toxicity (LOAEL), where compound **7i** demonstrated significantly lower toxicity compared to the other two compounds, making it a favourable choice. Additionally, other toxicity parameters showed marginal differences, warranting further comparison and analysis [39]. Compound **7i** displayed a moderate level of absorption and distribution. The metabolic profiles of all five compounds were essentially similar. Although

7j exhibited the highest total clearance value, **7i** also demonstrated a commendable value of 0.504 log ml/min/kg, indicating favourable excretion properties. A comprehensive summary of these results is provided in **Tables 3, 4, and 5**.

Compounds	Absorption							Distribution			
	Water solubility (log mol/L)	Caco2 permeability (log Papp in 10^{-6} cm/s)	Intestinal absorption (human) (% Absorbed)	Skin Permeability (log Kp)	P-glycoprotein substrate	P-glycoprotein I inhibitor	P-glycoprotein II inhibitor	VDss (human) (log L/kg)	Fraction unbound (human) (Fu)	BBB permeability (log BB)	CNS permeability (log PS)
7a	-2.384	1.135	89.624	-2.734	No	No	No	0.299	0.454	0.181	-2.293
7e	-2.724	1.134	89.18	-2.893	No	No	No	0.315	0.475	0.299	-2.925
7f	-2.696	-0.069	80.687	-2.764	Yes	No	No	0.158	0.358	-0.843	-2.526
7i	-2.58	1.132	89.738	-2.738	No	No	No	0.309	0.472	0.147	-2.86
7j	-2.793	0.951	90.674	-2.902	No	No	No	0.406	0.493	-0.757	-2.952

Table 3. ADMET analysis: Absorption and Distribution results of novel synthesized pyrazole Schiff base compounds.

Compounds	Metabolism							Excretion	
	CYP2D6 substrate	CYP3A4 substrate	CYP1A2 inhibitior	CYP2C19 inhibitior	CYP2C9 inhibitior	CYP2D6 inhibitior	CYP3A4 inhibitior	Total Clearance (log ml/min/kg)	Renal OCT2 substrate
7a	No	No	Yes	No	No	No	No	0.503	No
7e	No	No	Yes	No	No	No	No	0.247	No
7f	No	No	Yes	No	No	No	No	0.505	No
7i	No	No	Yes	No	No	No	No	0.504	No
7j	No	No	Yes	No	No	No	No	0.556	No

Table 4: ADMET analysis: Metabolism and Excretion results of novel synthesized pyrazole Schiff base compounds.

Compounds	Toxicity									
	AMES toxicity	Max. tolerated dose (human) (log mg/kg/day)	hERGI inhibitor	hERGII inhibitor	Oral Rat Acute Toxicity (LD50) (mol/kg)	OralRat Chronic Toxicity (LOAEL) (log mg/kg_bw/day)	Hepatotoxicity	Skin Sensitisation	T.Pyriformis toxicity (log ug/L)	Minnow toxicity (log mM)
7a	Yes	0.197	No	No	2.476	0.817	No	No	0.434	2.507
7e	No	0.293	No	No	2.339	1.389	No	No	0.467	2.382
7f	Yes	0.501	No	No	3.041	2.027	No	No	0.751	2.077
7i	No	0.317	No	No	2.479	0.78	No	No	0.471	2.498
7j	No	0.34	No	No	2.384	1.281	No	No	0.363	2.258

Table 5. ADMET analysis: Toxicity results of novel synthesized pyrazole Schiff base compounds.

D. Molecular Docking

To support the results of the in vitro biological assays, we conducted a detailed molecular docking analysis for compounds **7a**, **7e**, **7f**, **7i**, and **7j** to evaluate their binding affinity toward the crucial bacterial resistance protein, Penicillin G Acyl-Penicillin Binding Protein (PBP2a). This protein, derived from MRSA strain 27r, has been structurally resolved at a 2.45 Å resolution. It plays a central role in MRSA's resistance mechanism by maintaining its transpeptidase activity even in the presence of β-lactam antibiotics, due to its markedly low affinity for these drugs [40]. As a result, PBP2a bypasses the inhibitory effects on conventional penicillin-binding proteins, sustaining cell wall synthesis and conferring high-level resistance. Using the crystal structure (PDB ID: 1MWT), all five ligands were docked into the active site of PBP2a, and their docking scores were compared. Among them, compound **7i** showed the strongest interaction, with a docking energy of -7.4 kcal/mol, indicating a more stable and favorable binding than the other analogs (**Fig. 2**) [41]. This result positions compound **7i** as a promising candidate for further development as an anti-MRSA agent [42].

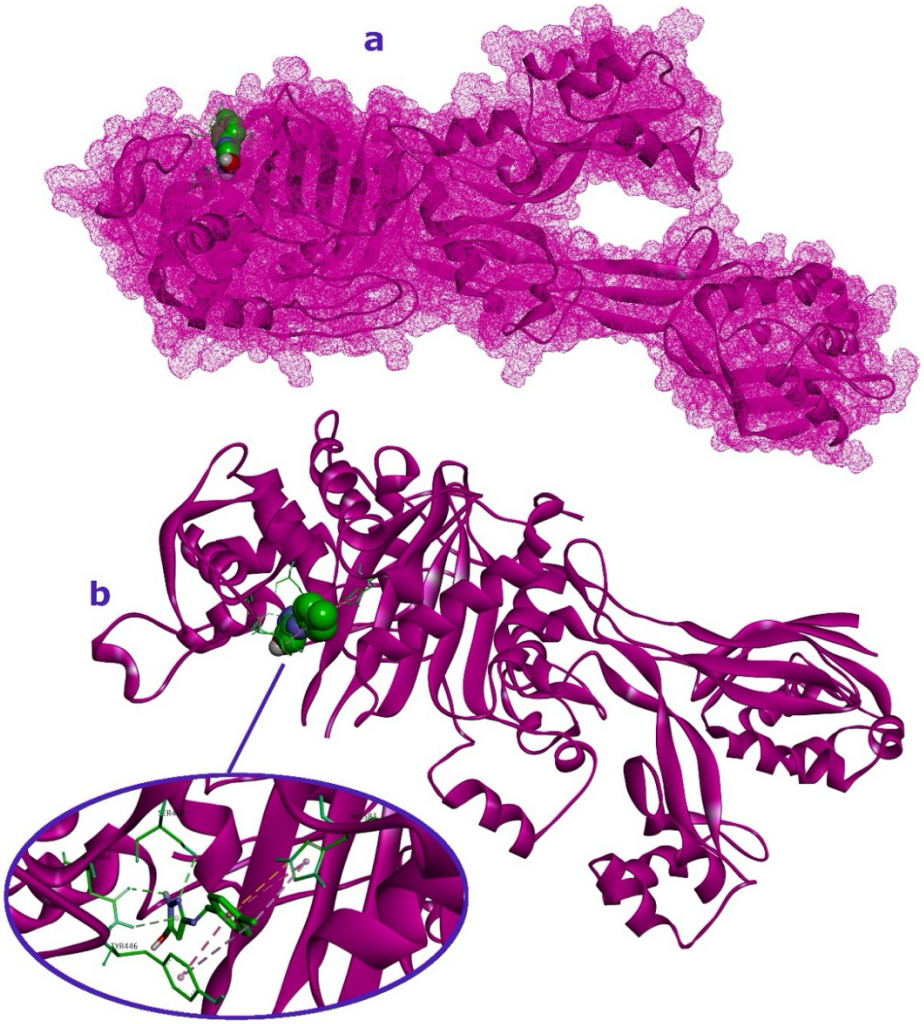

Fig. 2. Molecular docking: (a) surface and (b) cartoon model representation of the targeted protein, where the **7i molecule** is bound inside the active site.

To examine the nature of the binding in more detail, especially for compound **7i**, we analyzed the docking results using Discovery Studio Visualizer, which provided clear surface and cartoon representations of the protein-ligand complex **(Fig. 2)**. The ligand was well accommodated within the binding pocket of the receptor, with its pyrazole ring and benzene centroid playing a significant role in the interaction. Notably, the nitrogen atoms of the pyrazole unit formed hydrogen bonds with two key residues: ASN464 and SER462, with bond

distances of 2.34 Å and 2.91 Å, respectively. These bonds were mediated by the lone pairs and hydrogen atoms on the pyrazole's nitrogen, forming a highly stable interaction network, as shown in **Fig. 3** and detailed in **Table 6** [43]. Furthermore, TYR446 contributed additional stabilization through π–π T-shaped stacking and π–alkyl interactions with the benzene ring and methyl groups of the ligand **(Table 6; Fig. 3)** [44]. HIS583 also played a role in maintaining the ligand orientation through interactions with the same moiety. The combined influence of these hydrogen bonds, aromatic stacking, and hydrophobic interactions ensured that compound **7i** remained securely positioned in the active site throughout the simulation. This binding configuration was further validated through molecular dynamics simulations, which confirmed the robustness and persistence of the protein-ligand interactions over time.

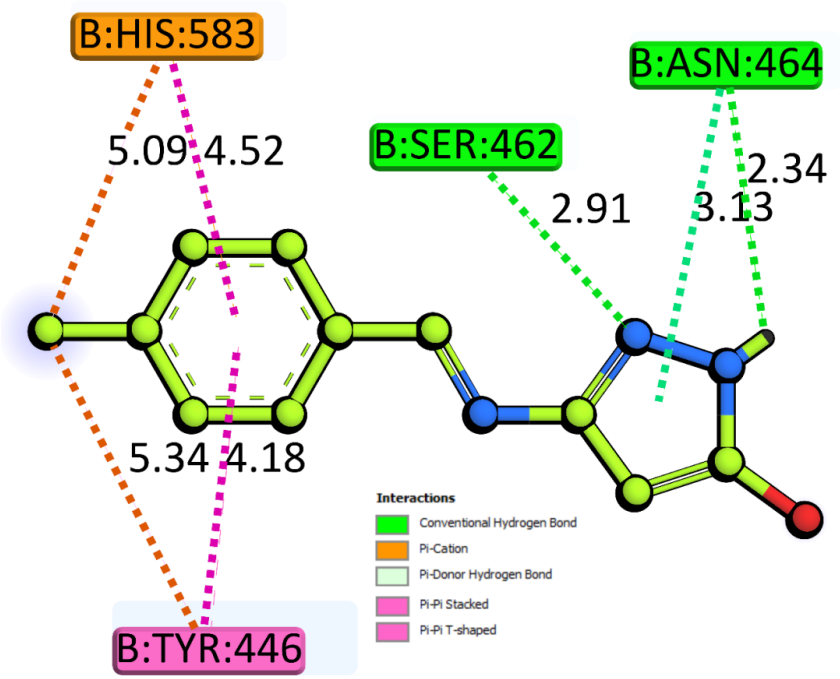

Fig. 3. 2D view of interactions between the 7i molecule and 1MWT protein.

PDB ID	Residue	Ligand	Interaction Type	Distance
1MWT	ASN464	Pyrazole NH	Conventional hydrogen bond	2.34
	ASN464	Pyrazole nitrogen	π-donor hydrogen bond	3.13
	SER462	Centroid of the pyrazole ring	Conventional hydrogen bond	2.91
	TYR446	Centroid of benzene ring	π-π T-shaped	4.18
	TYR446	CH_3 carbon	π-carbon	5.34
	HIS583	Centroid of benzene ring	π- π carbon	4.52
	HIS583	CH_3 carbon	π-carbon	5.09

Table 6. Detailed amino acid residue-ligand interactions in the active site of the protein.

E. Molecular Dynamics Simulation

To investigate the conformational integrity and dynamic behavior of the protein–ligand complex, a 100ns molecular dynamics (MD) simulation was conducted using the PBP2a protein and the 7i molecule as the interacting system. This long-term simulation was designed to mimic physiological conditions, enabling a comprehensive evaluation of the complex's structural stability and binding interactions over time. A central parameter examined during the simulation was the Root Mean Square Deviation (RMSD), which served as a measure of how much the atomic positions of the protein and ligand fluctuated relative to their initial conformation [45]. Beyond structural displacement, special attention was paid to the quality and consistency of intermolecular interactions, including hydrogen bonding, π–π stacking, and hydrophobic forces, which are essential in sustaining the ligand's occupancy within the active site [46]. These analyses provided critical insights into the stability of the interaction throughout the simulation period. A detailed visual breakdown of these metrics is provided in **Fig. 4**, which highlights the structural and dynamic attributes of the complex. The results reinforce the conclusion that compound 7i maintains a stable and bioactive binding mode with PBP2a.

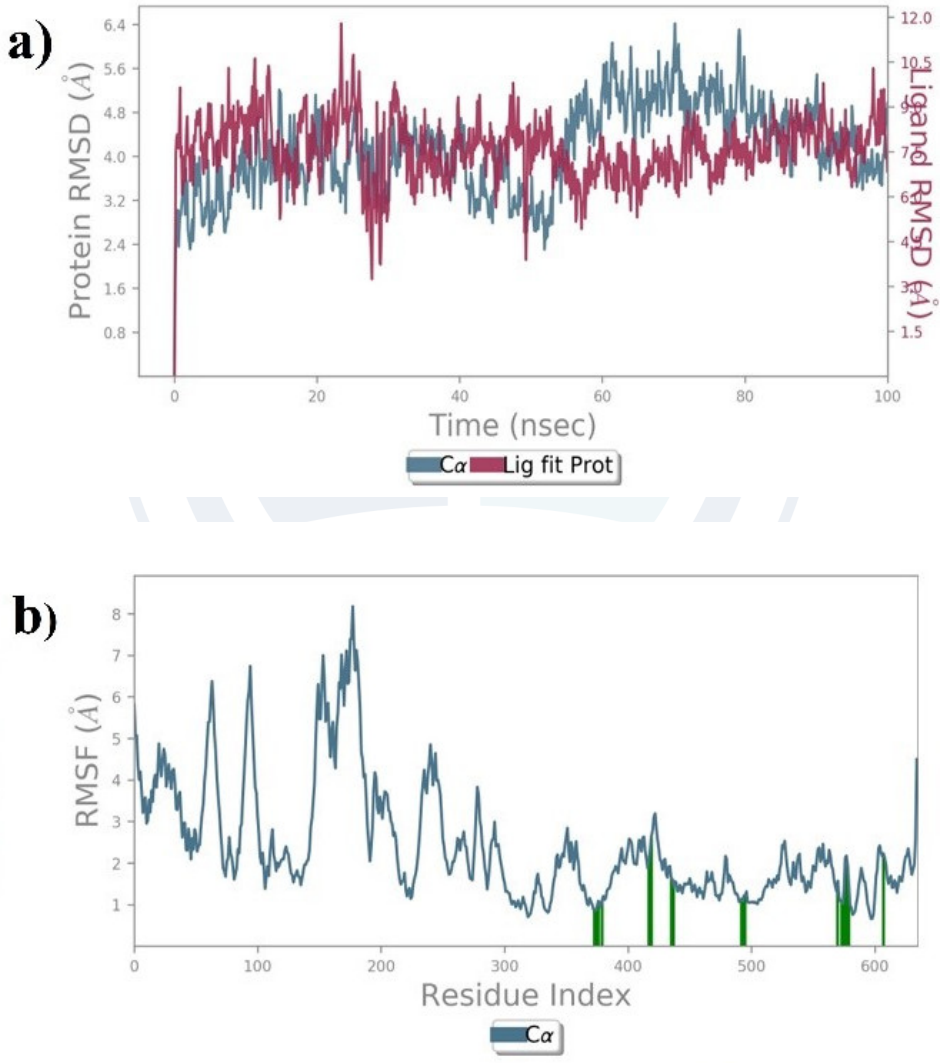

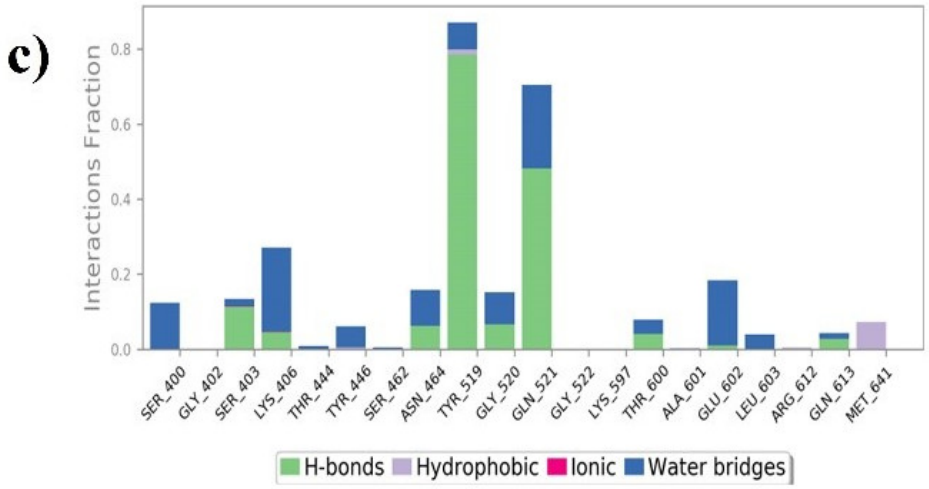

Fig. 4. (a) RMSD of protein and ligand, (b)RMSF of protein, and (c) Fingerprints of protein-ligand interactions during the simulations.

As illustrated in **Fig. 4a**, the RMSD profile shows the time-dependent structural changes for both the ligand and the protein across the 100 ns simulation. Compound 7i displayed an initial adjustment phase before stabilizing in the binding pocket, maintaining an average deviation of approximately 3.9 Å, indicating successful accommodation within the active site [47]. On the other hand, the PBP2a protein underwent a short equilibration period during the first 20 ns, after which its conformation remained largely stable, with RMSD values ranging between 2.4 and 5.8 Å. This steady behavior suggests minimal global structural fluctuations. Further investigation using Root Mean Square Fluctuation (RMSF), presented in **Fig. 4b**, revealed that the residue-level flexibility ranged from 1 to 7 Å, with most active site residues showing fluctuations below 3 Å, pointing to their rigid and well-maintained structure. These observations jointly confirm that compound **7i** remained securely bound within the active site. In contrast, the protein structure remained conformationally stable, reinforcing the overall robustness of the complex under simulated physiological conditions [48].

A more detailed analysis of ligand–receptor interactions was performed using interaction fingerprint mapping, as shown in **Fig. 4c**. This analysis revealed the persistence of several critical hydrogen bonds formed by **7i** with key residues of PBP2a, specifically SER462, ASN464, TYR519, GLY520, and GLN521. Among these, ASN464 and SER462 were particularly significant, forming stable hydrogen bonds with the pyrazole nitrogen of **7i** for approximately 93% and 70% of the simulation duration, respectively. These interactions played a foundational role in anchoring the ligand in the binding pocket. Additionally, TYR519 and GLY520 contributed to binding stability through hydrophobic contacts and water-mediated bridging interactions. Together, these long-lived, cooperative interactions exemplify the complex network of non-covalent forces that preserve the spatial arrangement of the ligand during simulation. Overall, the results highlight the crucial role of hydrogen bonding and hydrophobic interactions in maintaining a dynamically stable and specific binding between 7i and the PBP2a protein.

F. Molecular Mechanics Generalized Born Surface Area (MM-GBSA)

MM-GBSA analysis was used to assess the binding free energy between compound **7i** and the target protein [49]. This calculation was carried out by analyzing the MD simulation trajectory over a 100 ns period, with MM-GBSA analysis conducted for each frame at 10 ns intervals. The complex structure of **7i**-PBP2a underwent a thorough examination, revealing a notably negative net binding free energy of -42.81kcal/mol [50]. This suggests a substantial contribution of the binding free energy to the stability of the complex.

Consequently, the favorable energetics of the **7i**-PBP2a interaction are pivotal for maintaining complex stability (**Fig. 5**).

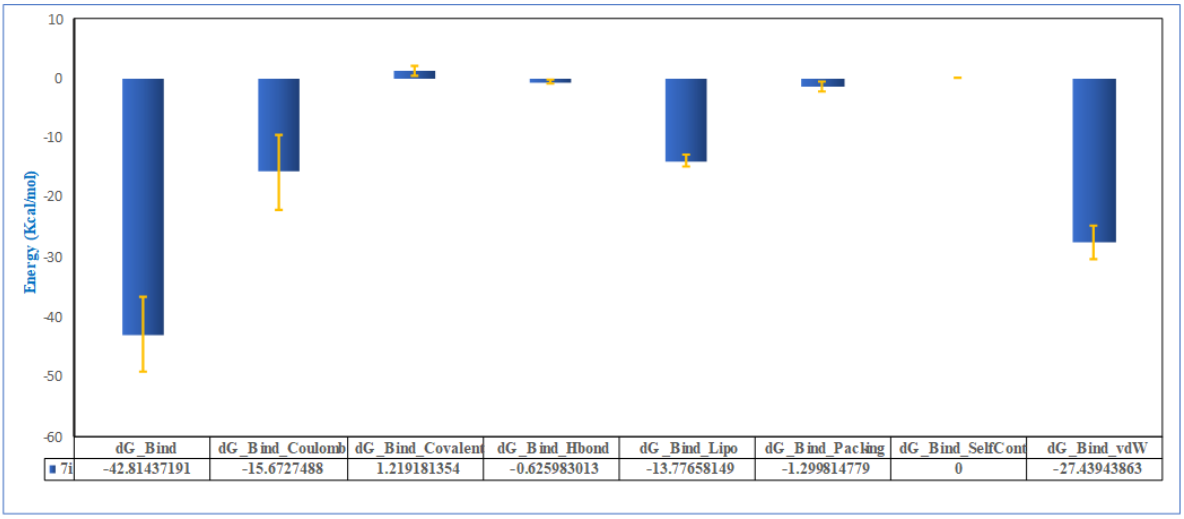

Fig. 5. Evaluated MM-GBSA binding energies for the 7i-PBP2a complex.

G. Molecular Geometry Optimization of Compound 7i

To understand the electronic configuration and charge distribution of compound **7i** at a quantum chemical level, we employed Density Functional Theory (DFT) calculations using Gaussian 16 software, applying the B3LYP/6-311+G(d,p) basis set. The optimized molecular structure, shown in **Fig. 6a**, reveals the spatial arrangement and geometrical parameters critical for its electronic behavior. Further insight was obtained through the Molecular Electrostatic Potential (MEP) map, depicted in **Fig. 6b**, which displays zones of varying electron density across the molecular surface. The analysis shows that positive electrostatic potential is concentrated on the pyrazole NH group and its adjacent hydrogen atoms, indicating regions susceptible to nucleophilic attack or electron acceptance. Conversely, electron-rich domains were observed at the pyrazole nitrogen lone pair and benzene ring centroid, serving as electron donor sites. These features underscore the internal polarity of the molecule and highlight areas likely to engage in intermolecular interactions [51].

In parallel, the Frontier Molecular Orbitals (FMOs), including the Highest Occupied Molecular Orbital (HOMO) and Lowest Unoccupied Molecular Orbital (LUMO), were visualized to evaluate the molecule's charge transfer potential. As illustrated in **Fig. 6**, the HOMO and LUMO orbitals are rendered in three-dimensional form with lobes marked in pink and green, representing their positive and negative phases, respectively. The computed HOMO–LUMO energy gap was determined to be 4.283 eV **(Fig. 7)**, indicating a relatively wide band gap that reflects strong chemical stability and suggests good electron transfer properties [52]. The electron density in the HOMO was primarily distributed over the pyrazole unit, the C=N double bond in the Schiff base, and parts of the benzene rings. In contrast, the LUMO density was more localized around the central benzene core. This spatial separation suggests that electron excitation would involve charge redistribution between these distinct π-conjugated regions, relevant for applications involving optical or redox activity.

To further characterize the chemical reactivity of compound 7i, a series of global descriptors was calculated based on orbital energy values, and the results are summarized in **Table 7**. These include the electrophilicity index (ω), chemical potential (ν), global hardness (η), and softness (s). The recorded EHOMO and ELUMO values suggest that the molecule could support photoactive or biologically relevant electronic transitions. Specifically, the compound showed a low global hardness of 2.141 eV, paired with a highly negative chemical potential of -3.873 eV, indicating that it is a soft and highly polarizable molecule. Moreover, the

electronegativity and electrophilicity index measured at 3.873 eV and 3.502 eV, respectively, reflect the molecule's strong electron-withdrawing capacity, suggesting its potential as an electrophilic species capable of participating in biological targeting or catalytic transformations [53].

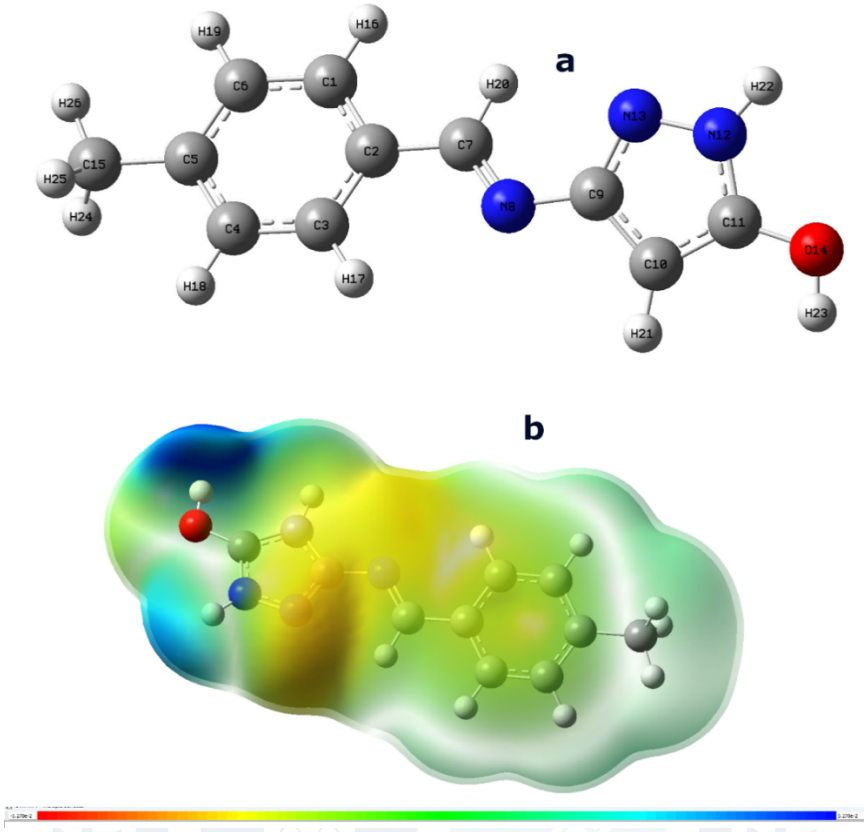

Fig. 6. (a) 3-dimensional DFT geometry optimized electronic structure and (b) Molecular electrostatic potential plot of 7i compound.

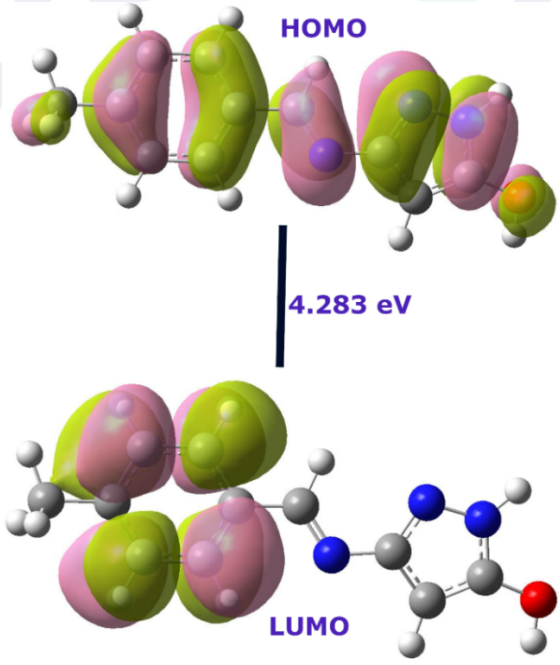

Fig. 7. Three-dimensional plots of the HOMO and LUMO of 7i with their energy gap value.

Parameter	Molecule value
E_{HOMO} (eV)	-6.015
E_{LUMO} (eV)	-1.731
Energy gap (ΔE) (eV)	4.283
Ionization potential (IP) (eV)	6.015
Electron affinity (EA) (eV)	1.731
Electronegativity (χ) (eV)	3.873
Chemical potential (μ) (eV)	-3.873
Global Hardness (η) (eV)	2.141
Softness(σ) (eV^{-1})	0.466
Global Electrophilicity (ω) (eV)	3.502

Table 7. Global chemical reactivity descriptors of the 7i molecule calculated using DFT at the B3LYP/6-311+G(d,p) level of theory.

H. Antibacterial Studies

- **MIC Assay**

The minimum inhibitory concentration (MIC) values of the synthesized pyrazole Schiff base compounds against MRSA are presented in Table 8. The results demonstrate that antibacterial activity is influenced by the nature of the substituents on the benzylidene moiety. Compounds with electron-withdrawing groups, such as the nitro group in 7f and the fluoro group in 7e, showed the lowest MIC values, indicating stronger antibacterial activity [54]. In contrast, compounds with electron-donating groups, such as the methyl group in 7i and the methoxy group in 7j, exhibited comparatively higher MIC values, while the unsubstituted derivative 7a also showed reduced potency. Overall, the MIC study highlights a clear structure–activity relationship, where electron-withdrawing substituents enhance antibacterial potency, whereas electron-donating or unsubstituted systems result in moderate to weak activity.

Compound	MIC (μg/mL)
7a	92
7e	75
7f	71
7i	84
7j	96

Table 8. MIC values for synthesized triazoline compounds

- **Zone of Inhibition Assay**

Clindamycin, an antibiotic used as a standard at 100 μg in the zone inhibition assay against the MRSA strain, had a zone of inhibition of 16 mm, indicating slight resistance to MRSA. In contrast, the control sample, which contained only DMSO, showed no inhibition. Compound **7i** exhibited different responses at various concentrations. It showed no inhibition at two concentrations: 25 μg and 50 μg, but resulted in an inhibition

zone of diameter measuring about 10mm when used at 100 µg (**Fig. 8**); this moderate inhibitory effect indicates its effectiveness against MRSA's replication process.

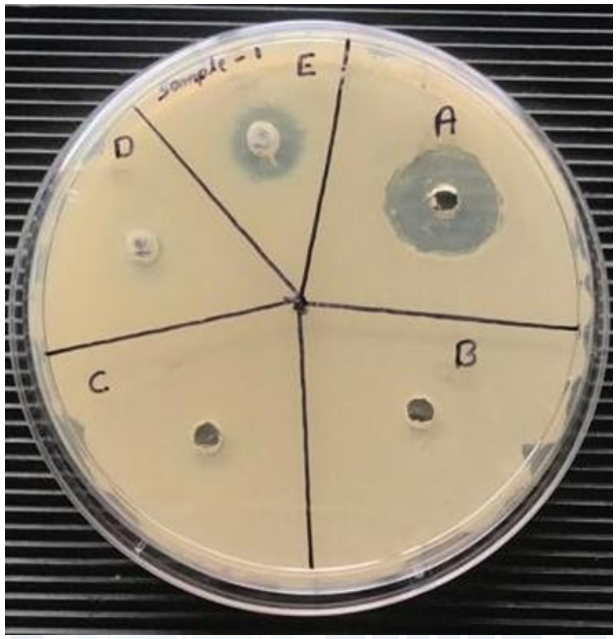

Fig. 8. Zone of inhibition assay of compound 7i against MRSA strain: A- Standard (Clindamycin; 50µg/well), B- Control (DMSO), C- Sample (25µg /well), D-Sample (50µg /well), E- Sample (100µg/well).

IV. Conclusion

In this study, a series of pyrazole Schiff bases was designed and synthesized for their potential antibacterial activity against MRSA. Structural characterization was confirmed by FT-IR, ^{1}H NMR, ^{13}C NMR, and elemental analysis, which validated the successful formation of the imine (C=N) group and the expected substitution patterns in the synthesized derivatives. These spectral results provided strong evidence for the purity and correct structure of the compounds. Utilizing a comprehensive approach that encompassed pharmacophore modeling, ADMET screening, molecular docking, molecular dynamics simulations, and Density Functional Theory calculations, compound 7i emerged as a promising candidate. It exhibited high binding affinity and favourable pharmacokinetic properties, making it a valuable lead compound. Detailed analysis of the protein-ligand interactions underscored the significance of hydrogen bonding and hydrophobic interactions in stabilizing the complex, while molecular dynamics simulations confirmed its stability. Electronic structure and reactivity analysis revealed 7i's favourable stability, softness, and electrophilic nature, supporting its potential as a drug candidate. The combined spectral, computational, and biological findings identify compound 7i as a promising scaffold for combating antibiotic-resistant MRSA strains, warranting further optimization and development in the fight against resistant pathogens.

V. Credit Authorship Contribution Statement

K.B. Chethan Kumar: Writing – review & editing, Writing – original draft, Software, Methodology. **Prabhudeva B.B:** Writing – review & editing. **Y.B. Basavaraju:** Writing – review & editing, Supervision, Data curation.

VI. Declaration of Competing Interest

The authors declare no competing interests.

VII. Acknowledgment

The authors received no financial support for the research.

VIII. Funding

The authors declare that they received no funds, grants, or other support.

IX. Data Availability Statement

All data generated or analysed during this study are included in this published article.

X. Clinical trial number

Not applicable

XI. Consent to Publish declaration

Not applicable

XII. Consent to Participate declaration

Not applicable

XIII. Ethics declaration

Not applicable

XIV. References

[1] C. P. Harkins *et al.*, "Methicillin-resistant Staphylococcus aureus emerged long before the introduction of methicillin into clinical practice," *Genome Biol*, vol. 18, no. 1, Dec. 2017, doi: 10.1186/s13059-017-1252-9.

[2] R. Sultana *et al.*, "Synthesis, spectral characterization of pyrazole derived Schiff base analogs: molecular dynamic simulation, antibacterial and DNA binding studies," *Journal of Biomolecular Structure and Dynamics*, vol. 41, no. 23, pp. 13724–13751, Dec. 2023, doi: 10.1080/07391102.2023.2179541.

[3] M. Lobanovska and G. Pilla, "Penicillin's Discovery and Antibiotic Resistance: Lessons for the Future?," *Yale J Biol Med*, vol. 90, no. 1, pp. 135–145, Mar. 2017.

[4] S. Nanjundaswamy *et al.*, "Design, synthesis, and in-silico studies of pyrazolylpyridine analogues: A futuristic antibacterial contender against coagulase positive superbug-MRSA," *Journal of Molecular Structure*, vol. 1255, p. 132400, May 2022, doi: 10.1016/j.molstruc.2022.132400.

[5] "Worldwide Epidemiology and Antibiotic Resistance of Staphylococcus aureus," in *Current Topics in Microbiology and Immunology*, Cham: Springer International Publishing, 2016, pp. 21–56. doi: 10.1007/82_2016_3.

[6] H. A. Grema, "Methicillin Resistant Staphylococcus aureus (MRSA): A Review," *Adv. Anim. Vet. Sci.*, vol. 3, no. 2, pp. 79–98, 2015, doi: 10.14737/journal.aavs/2015/3.2.79.98.

[7] H. Naeimi, Z. Sadat Nazifi, S. Matin Amininezhad, and M. Amouheidari, "Synthesis, characterization and in vitro antimicrobial activity of some new Schiff bases and their complexes," *J Antibiot*, vol. 66, no. 11, pp. 687–689, Nov. 2013, doi: 10.1038/ja.2013.73.

[8] M. Coandă, C. Limban, and D. C. Nuță, "Small Schiff Base Molecules—A Possible Strategy to Combat Biofilm-Related Infections," *Antibiotics*, vol. 13, no. 1, p. 75, Jan. 2024, doi: 10.3390/antibiotics13010075.

[9] R. Verma *et al.*, "Pyrazole-based analogs as potential antibacterial agents against methicillin-resistance staphylococcus aureus (MRSA) and its SAR elucidation," *European Journal of Medicinal Chemistry*, vol. 212, p. 113134, Feb. 2021, doi: 10.1016/j.ejmech.2020.113134.

[10] A. S. Hassan, G. O. Moustafa, A. A. Askar, A. M. Naglah, and M. A. Al-Omar, "Synthesis and antibacterial evaluation of fused pyrazoles and Schiff bases," *Synthetic Communications*, vol. 48, no. 21, pp. 2761–2772, Nov. 2018, doi: 10.1080/00397911.2018.1524492.

[11] N. M. Morsy, A. S. Hassan, T. S. Hafez, M. R. H. Mahran, I. A. Sadawe, and A. M. Gbaj, "Synthesis, antitumor activity, enzyme assay, DNA binding and molecular docking of Bis-Schiff bases of pyrazoles," *J IRAN CHEM SOC*, vol. 18, no. 1, pp. 47–59, Jan. 2021, doi: 10.1007/s13738-020-02004-y.

[12] M. Abdel-Aziz, G. E.-D. A. Abuo-Rahma, and A. A. Hassan, "Synthesis of novel pyrazole derivatives and evaluation of their antidepressant and anticonvulsant activities," *European Journal of Medicinal Chemistry*, vol. 44, no. 9, pp. 3480–3487, Sep. 2009, doi: 10.1016/j.ejmech.2009.01.032.

[13] D. D. C. Malvar *et al.*, "Antinociceptive, anti-inflammatory and antipyretic effects of 1.5-diphenyl-1H-Pyrazole-3-carbohydrazide, a new heterocyclic pyrazole derivative," *Life Sciences*, vol. 95, no. 2, pp. 81–88, Jan. 2014, doi: 10.1016/j.lfs.2013.12.005.

[14] M. Abdel-Aziz, G. E.-D. A. Abuo-Rahma, and A. A. Hassan, "Synthesis of novel pyrazole derivatives and evaluation of their antidepressant and anticonvulsant activities," *European Journal of Medicinal Chemistry*, vol. 44, no. 9, pp. 3480–3487, Sep. 2009, doi: 10.1016/j.ejmech.2009.01.032.

[15] G. M. Morris *et al.*, "AutoDock4 and AutoDockTools4: Automated docking with selective receptor flexibility," *J Comput Chem*, vol. 30, no. 16, pp. 2785–2791, Dec. 2009, doi: 10.1002/jcc.21256.

[16] J. Eberhardt, D. Santos-Martins, A. F. Tillack, and S. Forli, "AutoDock Vina 1.2.0: New Docking Methods, Expanded Force Field, and Python Bindings," *J. Chem. Inf. Model.*, vol. 61, no. 8, pp. 3891–3898, Aug. 2021, doi: 10.1021/acs.jcim.1c00203.

[17] O. Trott and A. J. Olson, "AutoDock Vina: Improving the speed and accuracy of docking with a new scoring function, efficient optimization, and multithreading," *J Comput Chem*, vol. 31, no. 2, pp. 455–461, Jan. 2010, doi: 10.1002/jcc.21334.

[18] J. Jayaprakash *et al.*, "Phytochemicals of Citrus Fruits: The in-silico Investigation against Sars-CoV-2 Proteins," *Trends Sci*, vol. 20, no. 1, p. 3508, Nov. 2022, doi: 10.48048/tis.2023.3508.

[19] E. Bursal *et al.*, "Determination of Phenolic Content, Biological Activity, and Enzyme Inhibitory Properties with Molecular Docking Studies of *Rumex nepalensis*, an Endemic Medicinal Plant," *JFNR*, vol. 9, no. 3, pp. 114–123, Mar. 2021, doi: 10.12691/jfnr-9-3-3.

[20] J. Jayashankar *et al.*, "An in-silico investigation of volatile compounds in Tulsi and Ginger as a potent inhalant for SARS-CoV-2 treatment," *J IRAN CHEM SOC*, vol. 21, no. 2, pp. 479–502, Feb. 2024, doi: 10.1007/s13738-023-02939-y.

[21] S. Nanjundaswamy *et al.*, "Design, synthesis of pyridine coupled pyrimidinone/pyrimidinthione as anti-MRSA agent: Validation by molecular docking and dynamics simulation," *Journal of Biomolecular Structure and Dynamics*, vol. 40, no. 22, pp. 12106–12117, Dec. 2022, doi: 10.1080/07391102.2021.1968496.

[22] S. Nanjundaswamy *et al.*, "Pyridine coupled pyrazole analogues as lethal weapon against MRSA: An in-vitro and in-silico approach," *Microbial Pathogenesis*, vol. 166, p. 105508, May 2022, doi: 10.1016/j.micpath.2022.105508.

[23] S. Nanjundaswamy *et al.*, "Synthesis, crystal structure, in-silico ADMET, molecular docking and dynamics simulation studies of thiophene-chalcone analogues," *Journal of Molecular Structure*, vol. 1247, p. 131365, Jan. 2022, doi: 10.1016/j.molstruc.2021.131365.

[24] V. K. Sharma, P. P. Nandekar, A. Sangamwar, H. Pérez-Sánchez, and S. M. Agarwal, "Structure guided design and binding analysis of EGFR inhibiting analogues of erlotinib and AEE788 using ensemble docking, molecular dynamics and MM-GBSA," *RSC Adv.*, vol. 6, no. 70, pp. 65725–65735, 2016, doi: 10.1039/c6ra08517b.

[25] S. Nanjundaswamy *et al.*, "Design, synthesis, and in-silico studies of pyrazolylpyridine analogues: A futuristic antibacterial contender against coagulase positive superbug-MRSA," *Journal of Molecular Structure*, vol. 1255, p. 132400, May 2022, doi: 10.1016/j.molstruc.2022.132400.

[26] D. P. Prashanth, G. N. Ningaraju, S. Rangappa, K. S. Rangappa, and C. S. Karthik, "Exploring the potential of thiazole derivatives in modulating the Wnt/β-catenin pathway for colon cancer therapy," *Discov Mol*, vol. 2, no. 1, Jun. 2025, doi: 10.1007/s44345-025-00015-x.

[27] M. B, Y. D. Bodke, N. O, L. T. N, N. G, and S. Ma, "Coumarin-Benzothiazole Based Azo Dyes: Synthesis, Characterization, Computational, Photophysical and Biological Studies," *Journal of Molecular Structure*, vol. 1246, p. 131170, Dec. 2021, doi: 10.1016/j.molstruc.2021.131170.

[28] R. Manne and T. Åberg, "Koopmans' theorem for inner-shell ionization," *Chemical Physics Letters*, vol. 7, no. 2, pp. 282–284, Oct. 1970, doi: 10.1016/0009-2614(70)80309-8.

[29] M. S. Punith *et al.*, "2,4-difluorophenyl(piperidin-4-yl) methanoneoxime derivatives as potent contenders to combat antibacterial resistance of MRSA: In-silico approach," *Discov Mol*, vol. 2, no. 1, Jun. 2025, doi: 10.1007/s44345-025-00010-2.

[30] M. Balouiri, M. Sadiki, and S. K. Ibnsouda, "Methods for in vitro evaluating antimicrobial activity: A review," *Journal of Pharmaceutical Analysis*, vol. 6, no. 2, pp. 71–79, Apr. 2016, doi: 10.1016/j.jpha.2015.11.005.

[31] A. Alastruey-Izquierdo and M. Cuenca-Estrella, "EUCAST and CLSI: How to Assess in Vitro Susceptibility and Clinical Resistance," *Curr Fungal Infect Rep*, vol. 6, no. 3, pp. 229–234, Sep. 2012, doi: 10.1007/s12281-012-0100-3.

[32] S. M. Lee *et al.*, "Evaluation of the Broth Microdilution Method Using 2,3-Diphenyl-5-thienyl-(2)-tetrazolium Chloride for Rapidly Growing Mycobacteria Susceptibility Testing," *J Korean Med Sci*, vol. 22, no. 5, p. 784, 2007, doi: 10.3346/jkms.2007.22.5.784.

[33] M. G. Bergeron, J. L. Brusch, M. Barza, and L. Weinstein, "Bactericidal Activity and Pharmacology of Cefazolin," *Antimicrob Agents Chemother*, vol. 4, no. 4, pp. 396–401, Oct. 1973, doi: 10.1128/aac.4.4.396.

[34] N. Berber, "Synthesis of New Schiff Base Compounds and Identification of Their Structures," *Adıyaman University Journal of Science*, Jun. 2020, doi: 10.37094/adyujsci.633080.

[35] A. S. Abu-Surrah *et al.*, "New palladium(II) complexes bearing pyrazole-based Schiff base ligands: Synthesis, characterization and cytotoxicity," *European Journal of Medicinal Chemistry*, vol. 45, no. 2, pp. 471–475, Feb. 2010, doi: 10.1016/j.ejmech.2009.10.029.

[36] C. Feng, J.-J. Guo, L.-N. Sun, and H. Zhao, "Pyrazole Schiff bases cross-linked supramolecules: structural elucidation and antibacterial activity," *J IRAN CHEM SOC*, vol. 15, no. 12, pp. 2871–2876, Dec. 2018, doi: 10.1007/s13738-018-1473-1.

[37] R. Uthayamalar, N. Nivetha, and G. Ayyannan, "A New Pyrazolone Schiff Base: Synthesis, Characterization and Molecular Docking and Antioxidant Studies," *Chemical Science and Engineering Research*, vol. 1, no. 1, Aug. 2019, doi: 10.36686/ariviyal.cser.2019.01.01.004.

[38] S. A. Khan, A. M. Asiri, A. A. Basheike, and K. Sharma, "Green synthesis of novel pyrazole containing Schiff base derivatives as antibacterial agents on the bases of in-vitro and DFT," *Eur. J. Chem.*, vol. 4, no. 4, pp. 454–458, Dec. 2013, doi: 10.5155/eurjchem.4.4.454-458.784.

[39] N. Sharma, S. Parihar, R. N. Jadeja, R. Kant, and V. K. Gupta, "Crystal structure of (*Z*)-1-(3,4-dichlorophenyl)-3-methyl-4-[(naphthalen-1-ylamino)(*p*-tolyl)methylidene]-1*H*-pyrazol-5(4*H*)-one," *Acta Crystallogr E Struct Rep Online*, vol. 70, no. 9, pp. o955–o956, Sep. 2014, doi: 10.1107/s1600536814017140.

[40] Y.-F. Sun, F.-Y. Zhang, Y. Liu, Z.-Y. Wang, and X.-L. Cheng, "1,5-Dimethyl-4-[(*E*)-3-phenoxybenzylideneamino]-2-phenyl-1*H*-pyrazol-3(2*H*)-one," *Acta Crystallogr E Struct Rep Online*, vol. 64, no. 9, pp. o1679–o1679, Sep. 2008, doi: 10.1107/s1600536808024409.

[41] M.-A. Shalaby, E. Dokla, R. Serya, and K. Abouzid, "Identification of novel pyrazole and benzimidazole based derivatives as PBP2a inhibitors: Design, synthesis, and biological evaluation," *Archives of Pharmaceutical Sciences Ain Shams University*, vol. 3, no. 2, pp. 228–245, Jun. 2019, doi: 10.21608/aps.2019.16625.1010.

[42] P. Lavanya, S. Ramaiah, and A. Anbarasu, "A Molecular Docking and Dynamics Study to Screen Potent Anti-Staphylococcal Compounds Against Ceftaroline Resistant MRSA: IDENTIFICATIONOFANTI-MRSACOMPOUNDS," *J. Cell. Biochem.*, vol. 117, no. 2, pp. 542–548, Feb. 2016, doi: 10.1002/jcb.25307.

[43] K.-C. Hsu, Y.-F. Chen, and J.-M. Yang, "Binding Affinity Analysis of Protein-Ligand Complexes," in *2008 2nd International Conference on Bioinformatics and Biomedical Engineering*, Shanghai, China: IEEE, May 2008. doi: 10.1109/icbbe.2008.46.

[44] "The Foundations of Protein–Ligand Interaction," in *NATO Science for Peace and Security Series A: Chemistry and Biology*, Dordrecht: Springer Netherlands, 2009, pp. 79–101. doi: 10.1007/978-90-481-2339-1_6.

[45] I. Khosravi, M. Sahihi, H. A. Rudbari, G. Borhan, and Z. Chavoshpour-Natanzi, "The Interaction of a New Schiff Base Ligand with Human Serum Albumin: Molecular Docking and Molecular Dynamics Simulation Studies," *Journal of Macromolecular Science, Part B*, vol. 56, no. 9, pp. 636–643, Sep. 2017, doi: 10.1080/00222348.2017.1356634.

[46] K. Liu, E. Watanabe, and H. Kokubo, "Exploring the stability of ligand binding modes to proteins by molecular dynamics simulations," *J Comput Aided Mol Des*, vol. 31, no. 2, pp. 201–211, Feb. 2017, doi: 10.1007/s10822-016-0005-2.

[47] X. Hua, X. Du, and Z. Zhang, "Ligand binding and release investigated by contact-guided iterative multiple independent molecular dynamics simulations," *Chinese Journal of Chemical Physics*, vol. 34, no. 3, pp. 334–342, Jun. 2021, doi: 10.1063/1674-0068/cjcp2010181.

[48] "Molecular Dynamics Simulation Methods to Study Structural Dynamics of Proteins," in *Protein Folding Dynamics and Stability*, Singapore: Springer Nature Singapore, 2023, pp. 83–106. doi: 10.1007/978-981-99-2079-2_5.

[49] E. Wang *et al.*, "End-Point Binding Free Energy Calculation with MM/PBSA and MM/GBSA: Strategies and Applications in Drug Design," *Chem. Rev.*, vol. 119, no. 16, pp. 9478–9508, Aug. 2019, doi: 10.1021/acs.chemrev.9b00055.

[50] H. Karataş, H. K. Kiliç, B. Tüzün, and Z. Kökbudak, "Schiff base derivatives against monkeypox virus: Synthesis, in silico, MM-GBSA and SAR properties," *Journal of Molecular Structure*, vol. 1298, p. 137073, Feb. 2024, doi: 10.1016/j.molstruc.2023.137073.

[51] T. A. Nibila, T. K. S. Ahamed, P. P. Soufeena, K. Muraleedharan, P. Periyat, and K. K. Aravindakshan, "Synthesis, structural characterization, Hirshfeld surface and DFT based reactivity, UV filter and NLO studies of Schiff base analogue of 4-aminoantipyrine," *Results in Chemistry*, vol. 2, p. 100062, Jan. 2020, doi: 10.1016/j.rechem.2020.100062.

[52] Y.-X. Sun *et al.*, "Experimental and density functional studies on two structurally similar antipyrine derivatives: 4-(2-hydroxy-5-nitrobenzylidene-amino)-1,2-dihydro-1,5-dimethyl-2-phenylpyrazol-3-one and 4-(3-bromo-5-chloro-2-hydroxybenzylideneamino)-1,2-dihydro-1,5-dimethyl-2-phenylpyrazol-3-one," *Struct Chem*, vol. 17, no. 6, pp. 655–665, Dec. 2006, doi: 10.1007/s11224-006-9116-z.

[53] A. M. Naglah *et al.*, "Exploring the Potential Biological Activities of Pyrazole-Based Schiff Bases as Anti-Diabetic, Anti-Alzheimer's, Anti-Inflammatory, and Cytotoxic Agents: In Vitro Studies with Computational Predictions," *Pharmaceuticals*, vol. 17, no. 5, p. 655, May 2024, doi: 10.3390/ph17050655.

[54] F. Daemi, S. Allameh, and M. Pordel, "ChemInform Abstract: Synthesis and Biological Evaluation of Novel Pyrazole Derivatives as Antibacterial Agents.," *ChemInform*, vol. 44, no. 12, Mar. 2013, doi: 10.1002/chin.201312111.